**NTNU – Trondheim**
Norwegian University of
Science and Technology

# Measurements of Optical Parameters at Extraction from the Proton Synchrotron at CERN

Adrian Ulsrød

Master of Science in Physics and Mathematics
Submission date: March 2013
Supervisor: Morten Kildemo, IFY
Co-supervisor: Yannis Papaphilippou, CERN

Norwegian University of Science and Technology
Department of Physics

# Measurements of optical parameters at extraction from the Proton Synchrotron at CERN

Adrian Ulsrød

Norwegian University of Science & Technology

CERN, 10-1-001, CH-1211 Geneva 23, Switzerland

a.ulsroed@gmail.com

March 12, 2013



- Advisor (NTNU): Morten Kildemo
- Advisor (CERN): Yannis Papaphilippou

**Abstract**

This thesis concerns the reconstruction of a new set of extraction parameters from the Proton Synchrotron (PS) at CERN. The underlying data was taken from measurement campaigns held in 2012 and 2013, aquired using beam position monitors and screens in the TT2-TT10 line and in the SPS. The tools for reconstructing the dispersive and betatronic parameters are explained, and the difference in extraction parameters using two separate bump settings in the PS is investigated. Earlier findings are also used for comparison.

# Acknowledgements

There are many people who have assisted me in my technical studentship at CERN. At first I would like to express my thanks to my advisor Yannis Papaphilippou, who granted me the opportunity to come to CERN in the first place, as well as being an invaluable source of help when it comes to beam physics. It is to you I owe the most help. Yannis' colleague Hannes Bartosik also deserves my gratitude for asking good questions and helping out with troubleshooting.

My advisor back in Norway, Morten Kildemo was generous to act as my offical university advisor while I'm here at CERN. I offer you my thanks.

Many people have assisted me throughout the measurement runs. Antoine Lachaize deserves a shout-out for teaching me how to do the beam position measurements. Simone Gilardoni was playing the role of my technical guardian angel, filling in with his expertise when technical problems arose. Cedric Hernalsteens also provided me with useful input with his experience in the control room, as well as explaining me the details of the bump settings. Last but not least all of the PS and SPS operators deserve credit for always being present and helpful in the control room, 24/7.

Outside of the measurements I would like to thank Stephane Burger and Ana Guerrero for helping me out with the MTV systems and the somewhat nonintuitive .sdds file format. Special thanks to Massimo Giovannozzi for some useful input for the analysis. Finally, Elena Benedetto and Gianluigi Arduini have been instrumental in developing the theory for my thesis. Without you none of this would be possible!

Extra special thanks go out to my office mate Everton G. Souza and his colleague Mahboobeh Yarmohammadi Satri, who gave me some useful input on my thesis during the writing stage. You should know that it was much appreciated!

Adrian Ulsrød, March 2013

# Contents

# 1 Introduction

The LHC at CERN is dependent on a well-behaving accelerator complex in order to achieve the high performance requirements necessary for the physics experiments. Without properly matched optics in the components preceding the LHC, the quality of the beam will drop as tails in the particle distributions form. One such component is the TT2-TT10 transfer line, bridging the PS with the SPS.

To ensure proper beam transfer to the SPS, it is helpful to know the current state of the beam parameters (ie. dispersion, envelope and the slopes of the two) at extraction from the PS. In order to match the magnet strengths in the TT2-TT10 transfer line so that the beam goes safely between the PS and SPS orbits without blowups, these parameters have to be used as input. Hence, new measurement campaigns of the extraction parameters are necessary at regular intervals, especially before maintenance periods.

This thesis investigates the changes in the extraction parameters from the PS, with respect to earlier findings and methods in 2008 [2] and 2010 [3]. It is hypothesized that the parameters drift over time as changes are made upstream in the accelerator complex. Two measurement campaigns are dissected, one pertaining to dispersion measurements and another to beam profile measurements. The dispersion parameters $\{D, D'\}$ for two separate extraction conditions are calculated using numerical minimization, based on a least square error scheme in [2]. The envelope parameters $\{\alpha, \beta\}$ are then calculated, along with the emittance, using a similar scheme as with the dispersion. The analysis concludes that a drift has taken place, and presents an overview of the new parameters.

# 2 Materials and methods/Theory

## 2.1 Overview of the accelerator parts

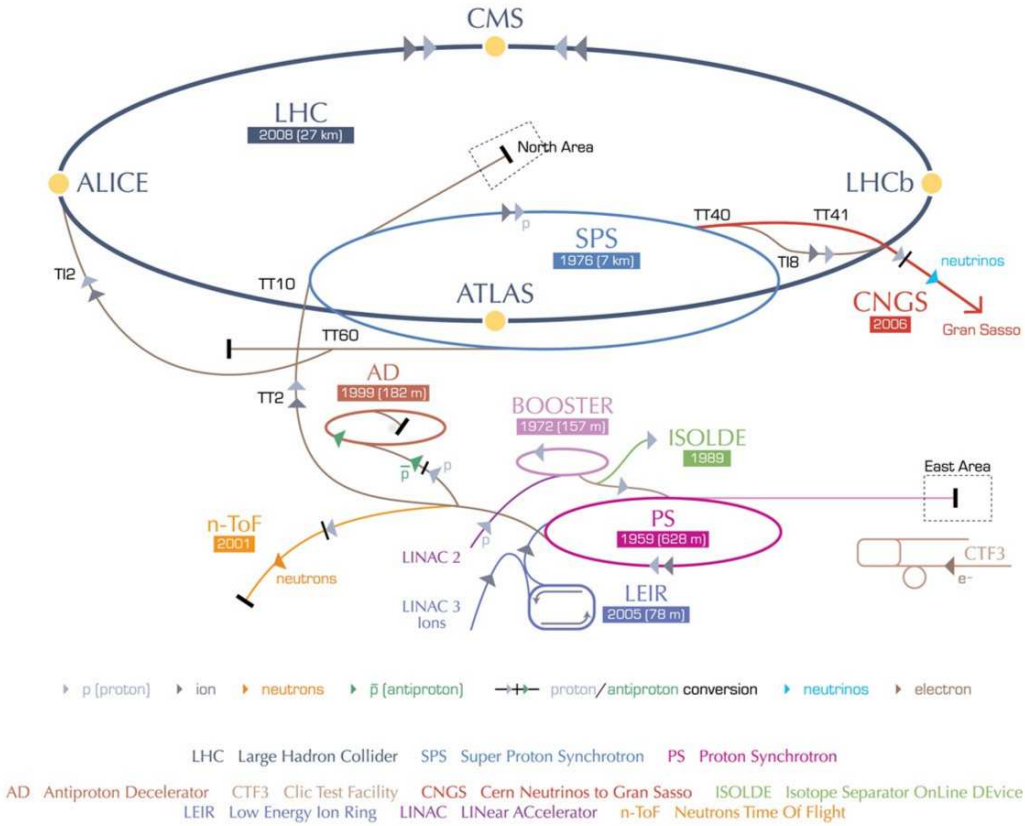


Figure 1: An overview of the accelerator complex at CERN.

Between each circular accelerator in the CERN accelerator complex (Figure 1), there is a transfer line which connects the two systems. The TT2-TT10 line is the transfer line between the PS and the SPS. This transfer line is documented in [13] and [6]. It is 1165 meters long and consists of two parts: The TT2 and the TT10 lines, 305 and 860 meters respectively.

The transfer line can be broken down into matching sections and FODO sections. The parts are listed in Table 1 in the order of beam passage. The FODO sections are there to replicate the conditions in the closest circular accelerator, in order to ease the transition from one system

to another. They consist of a recurring pair of two quadrupoles (two *families*) with equal but opposite effect, therefore causing a regular beating of the beam envelope in both planes. Meanwhile, the matching sections are groups of independent quadrupole magnets which can be used to modify the beam parameters $\{D, D', \alpha, \beta\}$ in each plane. They can be used to tailor the beam to each of the two FODO-sections, in order to prepare the beam for injection into the SPS so that the right injection conditions are satisfied.

The SPS is a synchrotron with a radius of 1100 meters [13]. It is the second largest circular accelerator at CERN, after the LHC. The PS is the third largest ring with a radius 11 times smaller than the SPS, at 100 meters.

| Accelerator part | Length [m] | Number of independent quadrupole families |
|---|---|---|
| PS | 628(1 turn) | 2 |
| TT2MS1 | 109 | 10 |
| TT2 FODO | 196 | 2 |
| TT10MS2 | 244 | 8 |
| TT10 FODO | 616 | 2 |
| SPS | 6912 (1 turn) | 2 |

Table 1: The accelerator parts relevant to this thesis, with lengths and the number of independent quadrupole families specified.

## 2.2 The extraction parameters

The goal of the transfer line is to make sure that the optical parameters of the passing beam change in a *controlled way* from one system to the next. These parameters are the *betatronic values* $\{\alpha, \beta\}$ as well as the *dispersion values* $\{D, D'\}$, which are separate along each transverse axis if one assumes no coupling.

From standard beam dynamics [15], one can find the relationship between these parameters. A particle $i$ in a longitudinal position $s$ in the accelerator complex has a transverse position given by:

$$x(s)_i = \beta(s)\epsilon_i \cos(\Delta\Psi(s) + \phi_i) + D(s)\left(\frac{p_i - p_0}{p_0}\right) \equiv x_{\beta,i}(s) + x_{D,i}(s), \quad (1)$$

where $\beta(s)$ is the betatronic function, $D(s)$ is the dispersion, $\Delta\Psi(s)$ is the accumulated phase and $p_0$ the ideal momentum, all related to the optics in the line. Meanwhile, the parameters that depend on the individual particle is the emittance $\epsilon_i$, the phase offset $\phi_i$ and the momentum $p_i$.

Averaging over all the particles in the beam for a given s, Equation 1 is reduced to

$$\overline{x(s)_i} \equiv x(s)_{BEAM} = \overline{x_{\beta,i}(s)} + D(s)\frac{\Delta p}{p} \tag{2}$$

where $\frac{\Delta p}{p}$ is the momentum spread of the beam as a whole, with respect to a reference momentum $p_0 \equiv p$. The left hand side is the average beam position, detectable by using *beam position monitors* (BPMs).

Hence, the change in beam position with respect to the momentum spread manifests as:

$$D(s) = \frac{\Delta(x(s)_{BEAM})}{\Delta\left(\frac{\Delta p}{p}\right)} \tag{3}$$

One can also use a formalism which emphasizes the *root mean square* (RMS) size of the beam instead of position. Assuming a Gaussian beam, one can take the RMS value of Equation 1 and obtain [2]:

$$\sigma_{RMS}(s)^2 = \beta(s)\epsilon_{RMS} + \left(D(s)\frac{\Delta p}{p}\right)^2. \tag{4}$$

where $\sigma_{RMS}(s)$ is the standard deviation of the measurable transverse beam size, $\epsilon_{RMS}$ is the corresponding standard deviation of the beam emittance.

The derivative of the dispersion with respect to longitudinal distance $s$ is dubbed $D'(s)$. The derivative of the beta function $\beta(s)$ is given by

$$\frac{\partial\beta(s)}{\partial s} \equiv -2\alpha(s). \tag{5}$$

Although the parameters $\{D, D', \alpha, \beta\}$ are defined by the structure of the line, they can differ from their ideal values because of changes in the upstream optics. These optical changes can occur when one or more magnets are changed, either by changing their position, replacing them or manipulating their gain.

By manually altering the optics in the transfer line with respect to the input/extraction parameters, one can engineer the desired output/injection parameters. One way to do this is to define a new set of magnet strengths/gains in the line, as their settings will directly alter the beam parameters. This can be done in order to match the design orbit of the downstream accelerator with its upstream counterpart. This is known as *matching* the line [13], and can be used to account for changes in the extraction conditions at the entrance of the line. Conversely, a badly matched line will cause the beam to blow up, causing beam losses and drops in the beam performance.

Two extraction conditions were used in the dispersion measurements discussed in this paper. They refer to two different bump settings for the extraction of LHC-type beams from the PS.

A *multi-turn extraction* method (MTE), implemented progressively in the PS since 2001 [11], is in its final commissioning phase. The test

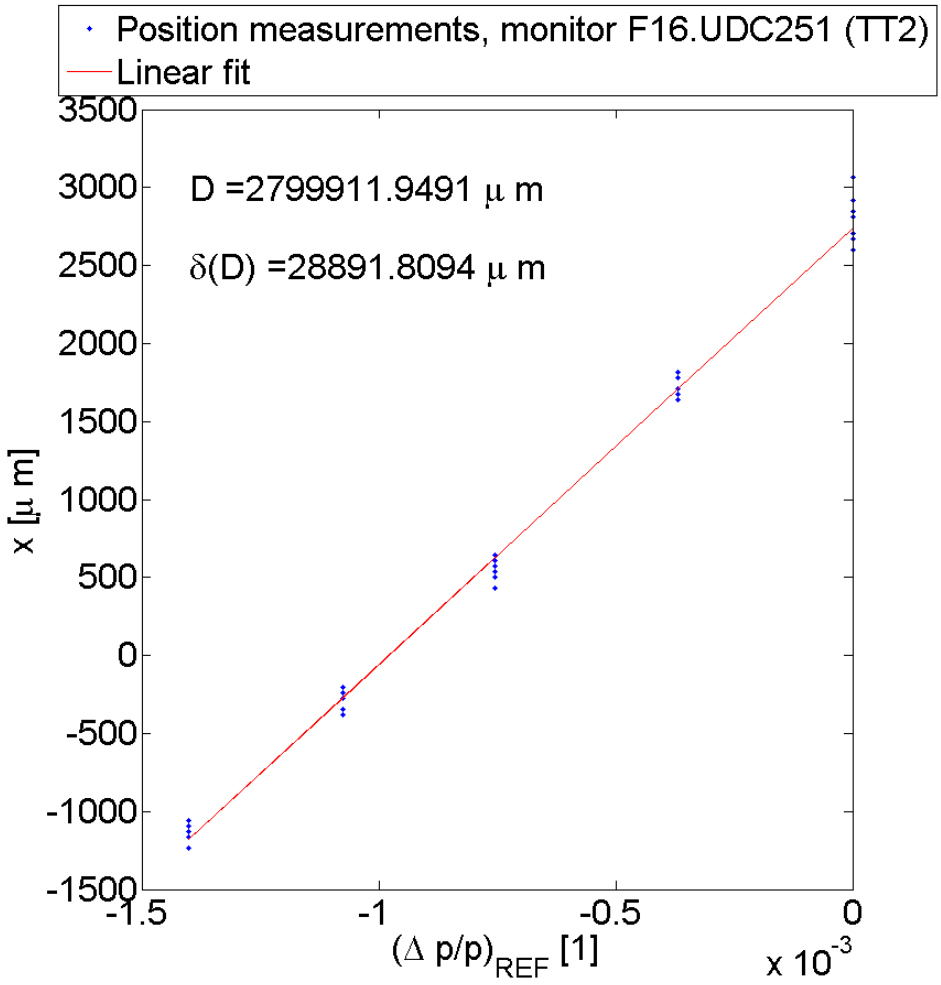


Figure 2: **An example of a dispersion calculation done for a single monitor in the horizontal plane, using beam position data as input.**

results show that the overall beam losses in the PS are reduced compared to the old extraction method. However, the losses are concentrated at the magnetic extraction septum, which guides the proton beams from the accelerator into the TT2-TT10 line.

In order to redistribute the losses so that the septum can last longer without maintenance, a shielded device known as a *dummy septum* will be placed upstream. This requires the orbit of the PS to be modified, as the high energy orbit correctors prior to extraction from the PS will have to be displaced to make room for the dummy septum. A different extraction bump setting is designed to counter this change in orbit, whose performance will be scrutinized in this thesis.

## 2.3 Dispersion measurements

### 2.3.1 Beam position monitors

BPMs can be found in both the TT2-TT10 line and the SPS. The distribution of monitors per accelerator section is listed in Table 2.

| Accelerator part | Number of BPMs, X | Number of BPMs, Y |
|---|---|---|
| TT2 | 6 | 6 |
| TT10 | 10 | 10 |
| SPS | 122(103*) | 113 (94*) |

Table 2: The total number of BPMs available in the TT2, TT10 and the first turn of the SPS. * refers to the monitors which only work in that plane.

These monitors were used to record the transverse beam position, by operating the application software *Yet Another Steering Program* (YASP) [9]. By recording the beam positions while varying the momentum spread, one can also exploit Equation 3 to obtain the dispersion at the location of the BPMs.

Note that depending on the location of the monitors, different instrumentation systems are used, resulting in differences in calibration. This discrepancy will be taken care of later using a dimensionless calibration factor $c_k$: $D_i \rightarrow c_k D_i$. $i$ refers to the dispersion location and $k$ the type of BPM at that location (the TT2, TT10 or the SPS). Furthermore, it is known [4] that most BPMs in the SPS only operate along one transverse axis, while the ones in TT2 and TT10 function along both axes (Table 2).

References [2] and [9] describe the procedure for calculating dispersion values using BPM measurements. The change in the synchrotron/RF frequency of the PS can modify the beam orbit, which in turn alters the momentum spread. The reference frequency is related to the momentum spread by the expression

$$\left(\frac{\Delta p}{p}\right)_{REF} = \frac{1}{\eta_{PS}} \left(\frac{\Delta f}{f}\right)_{REF}. \tag{6}$$

$(\Delta f/f)_{REF}$ is the relative change in RF frequency from a defined frequency $f_0$. $\eta_{PS}$ is the slippage factor at extraction from the PS:

$$\eta = \frac{1}{\gamma_{REL}^2} - \alpha_C \tag{7}$$

where $\gamma_{REL}$ is the relativistic gamma from special relativity, and $\alpha_C$ is the momentum compaction factor [15].

### 2.3.2 Dispersion measurement procedure

A measurement campaign with well defined beam settings was initiated on November 7th, 2012. The beam data is summarized in Table 3.

| Date | 07.11.12 |
|---|---|
| Beam type | 50 ns LHC-type |
| Kinetic energy [GeV] | 26 |
| Intensity [ppb] | $1.75 \cdot 10^{11}$ |
| $\epsilon_l$ [eVs] | 0.382 |
| $\epsilon_{NORM,X} \cong \epsilon_{NORM,Y}$ $[\mu mrad]$ | 1.6-1.7 |
| No. of bunches | 36 |
| Bunch rotation? | Yes |
| Momentum spread $\Delta p/p$ | $2.73 \cdot 10^{-4}$ |
| Error in momentum spread $\delta(\Delta p/p)$ | $1.8 \cdot 10^{-6}$ |

Table 3: Information on the beam used for the dispersion measurement campaign.

This beam was sent through the TT2-TT10 line and the SPS. Only the data from the first turn in the SPS are relevant for our dispersion mismatch and propagation analysis. The program *Beam Size Monitor* (BSM) calculated the momentum spread based on longitudinal profiles of the beam. Other values pertaining to the beam, such as the intensity and longitudinal emittance were aquired using this program.

The RF frequency sent from the SPS to the PS was varied in increments of 2 KHz at a time. This produced shifts in the frequency $(\Delta f/f)_{REF}$ in the PS, which in turn lead to a change in the momentum spread $\Delta p/p$ of the order of $3 \cdot 10^{-4}$.

Five different values of $\left(\frac{\Delta p}{p}\right)_{REF}$ were chosen per bump setting. For each value, at least 10 position measurements were obtained from each monitor.

### 2.3.3 Dispersion parameter calculation

Extracting the dispersion values required post-processing of the data. A Matlab script was written for easier data analysis, in order to tailor the output format. A plot of beam position as a function of momentum spread was produced for each monitor, bump setting and axis. The result was

a set of dispersion measurements $\{D_i\}$ and standard errors of the slope, $\{\delta(D_i)\}$, taken in both planes with both bump settings. Figure 2 shows an example of the calculation for one monitor.

A filtering process was then performed on the data sets, separately for each bump setting and axis choice. An error measure $E(D_i) \equiv |\delta(D_i)/D_i|$ was concieved to filter away the points with too high error bars relative to their values. A threshold of $E(D_i) < 3 \cdot \delta(E)$ was chosen, where $\delta(E)$ is the standard deviation in $\{E(D_i)\}$. All points above this threshold were removed from the analysis.

The procedure for the calculation of the extraction dispersion and its derivative is described in [2]. One starts by forming the *propagated dispersion*, named from the way it is modeled through a simulation of the optics in the software MAD-X [14]. It illustrates how the dispersion parameters at extraction from the PS propagates through the downstream optics:

$$D_{PROP,i} = C_i D_0 + S_i D'_0 + \tilde{D}_i. \tag{8}$$

$C_i$ and $S_i$ are the *cosine-* and *sinelike functions* which models how the dispersion parameters at the extraction point $i = 0$ are coupled with the parameters at point $i$. Their definitions are given in [15]:

$$C_i \equiv C(s_i, s_0) = \sqrt{\frac{\beta_i}{\beta_0}} \left(\cos(\mu_i - \mu_0) + \alpha_0 \sin(\mu_i - \mu_0)\right), \tag{9}$$

$$S_i \equiv S(s_i, s_0) = \sqrt{\beta_i \beta_0} \sin\left(\mu_i - \mu_0\right). \tag{10}$$

Here $\beta$ and $\alpha$ refer to the betatronic parameters, while $\mu$ denotes the *phase* at point $i$. MAD-X calculates these parameters for each point in the accelerator chain, using a modeled accelerator sequence as input.

An extra term $\tilde{D}_i$ is included in the propagated dispersion to account for changes in the dispersion that are *independent* of the initial dispersion conditions $\{D_0, D'_0\}$. Examples of accelerator elements that cause such changes [15] are kicker/dipole magnets.

A $\chi_D$-function is then constructed which represents the difference between the measured dispersion values and the propagated extraction parameters:

$$\chi_{D,m,n,k} = \sum_{i \in \{I_k\}} \left( \frac{c_{k,n} D_{MEAS,i,m,n} - D_{PROP,i,m,n}}{\sigma^2_{i,m,n}} \right)^2, \tag{11}$$

where $i$ runs over all monitors ($\{I_k\}$) for a given $k$, while $k$ denotes the monitor location (TT2, TT10 and the SPS). $n$ refers to the axis (X or Y) and $m$ pertains to the type of extraction condition used (old or new bump). The $c_k$-parameter is the *calibration factor* of each set of BPMs. $\sigma_i$ is the uncertainty of each monitor measurement, here defined to be the standard error of the dispersion $\delta(D_i)$.

One can then define the total square error:

$$\chi_D = \sum_{m=OLD,NEW}^{ex.cond.} \sum_{n=X,Y}^{axes} \sum_{k=TT2,\ldots,SPS}^{monitors} (\chi_{D,m,n,k}) \tag{12}$$

In order to find a local minima with reasonable values for the extraction parameters, Microsoft Excel's Solver tool was utilized. The applied algorithm was the GRG Nonlinear Engine [12], used for solving smooth nonlinear equations.

Reasonable limits on the target parameters were set, based on the results obtained in [2]. The limits are displayed in Table 4. Two constraints were not included in the table. These constraints were

- a maximum deviation of 20% between $c_{SPS,X}$ and $c_{SPS,Y}$,
- a minimum absolute threshold on the vertical dispersion parameters: $|D_{0,Y}| > 0.0001m$, $|D'_{0,Y}| > 0.0001$

The reasoning for the latter constraint was to avoid the trivial solution in the vertical plane of $(D_{0,Y}, D'_{0,Y}) = (0, 0)$.

| Parameter | Axis | Lower limit | Upper limit |
|---|---|---|---|
| $D_0$ [m] | X | 2 | 4 |
| $D'_0$ [1] | X | 0 | 0.5 |
| $D_0$ [m] | Y | -0.15 | 0.15 |
| $D'_0$ [1] | Y | -0.15 | 0.15 |
| $c_{TT2}$ [1] | Both | 0.7 | 1.3 |
| $c_{TT10}$ [1] | Both | 0.7 | 1.3 |
| $c_{SPS,X}$ [1] | X | 0.7 | 1.3 |
| $c_{SPS,Y}$ [1] | Y | 0.7 | 1.3 |

Table 4: The constraints on each output variable, when running Excel's Solver algorithm (GRG Nonlinear).

### 2.3.4 Error analysis of dispersion parameters

Minimizing Equation 12 with Excel is an effective method if one just wants to obtain the parameters which minimizes the expression, as one can set individual constraints for each variable. However the method does not provide *error measures* for the parameters. Therefore, a different method was also investigated.

$\chi_D$ can be minimized analytically by differentiating it with respect to each unknown dispersion and calibration factor, and setting each expression equal to zero. The result can be arranged into a set of linear equations. This provides the error in each parameter as a function of the terms in the inverse matrix.

The following analysis will provide an overview of the method, without descibing every element in each vector and matrix. A more thorough exposition is given in [2].

$$\left\{ \frac{\partial \chi_D(A_1, A_2, ...., A_{11}, A_{12})}{\partial A_l} = 0 \right\}, l \in \{1 - 12\} \tag{13}$$

$l$ refers to the variable which $\chi_D$ is differentiated upon. $l \in [1-8]$ refer to the dispersive parameters, and $l \in [9 - 12]$ are the calibration factors.

One can then set up a linear system:

$$\mathbf{M}\vec{x} = \vec{b}, \tag{14}$$

such that $\vec{x}$ is a vector of 12 unknowns: $\vec{x} = \{D_{0,newbump,X}, ..., c_{Y,SPS}\}^T$. $\vec{b}$ is a vector of constants and $\mathbf{M}$ is an invertible square matrix.

As it stands, solving Equation 14 for the unknowns in $\vec{x}$ will produce the *global minimum* of the system. However, as the variables have constraints as listed in Table 4, a local set of solutions has to be found. One way to achieve this is to perform a bifurcation of Equation 14 in two parts; one pertaining to calculating the dispersion values, and another to calculate the calibration factors. Then one can solve for the optimal set of dispersion parameters at extraction given a set of calibration factors, and vice verca.

The first invertible system with constraints is given by:

$$\mathbf{M}_{(D_0, D_0')}\vec{x}_{(D_0, D_0')} = \vec{b}_{(D_0, D_0')} - \sum_k c_k \vec{m}_{c_k}, \tag{15}$$

where $k$ runs over each calibration factor $c_k$. This system is identical to 14, except that the calibration factors $c_k$ are set as constant. This reduces the dimensionality of the system by 4. The constant terms are carried over to the right hand side of the equation, with $\vec{m}_{c_k}$ representing the elements in $\mathbf{M}$ which pertain to the calibration factor $c_k$. The subscript $(D_0, D_0')$ refers to the set of 8 dispersion parameters, as these are the unknowns in Equation 15.

Likewise, one can exchange the roles of the dispersion parameters and the calibration factors:

$$\mathbf{M}_c\vec{x}_c = \vec{b}_c - \sum_{m,n} D_{0,m,n}\vec{m}_{(D_{0,m,n})} - \sum_{m,n} D'_{0,m,n}\vec{m}_{(D'_{0,m,n})}, \tag{16}$$

where $m$ and $n$ run over all bump types and all axes respectively.

The result is two uncoupled invertible systems with fixed constraints. This ensures that one converges towards the local minimum aquired by Excel's GRG Nonlinear algorithm. One inserts the values calculated from Excel on the right hand side of Equations 15-16.

Matrix $\mathbf{M}$ in Equation 14 has the property [2] that it contains the errors in vector $\vec{x}$. They are given by the square root of the inverse elements. The same applies for the matrices $\mathbf{M}_c$ and $\mathbf{M}_{(D_0, D_0')}$ in Equations 15-16:

$$\delta(x_{(D_0,D_0'),l}) = \sqrt{M^{-1}_{(D_0,D_0')(l,l)}}, \tag{17}$$

$$\delta(x_{c,l}) = \sqrt{M^{-1}_{c(l,l)}} \tag{18}$$

where $l$ is the variable's position (element-wise) in the corresponding solution vectors $\vec{x}_c$ and $\vec{x}_{(D_0,D_0')}$. $(l,l)$ refers to the coordinates of the inverse matrix elements.

Using the Gaussian law of error propagation (Appendix A), one can also derive errors for both the fitted dispersion as well as the product of the measured dispersion and the corresponding calibration factor:

$$\delta(D_{PROP,i}) = \sqrt{C_i^2(\delta D_0)^2 + S_i^2(\delta D_0')^2}, \tag{19}$$

$$\delta(c_k D_{MEAS,i}) = c_k D_{MEAS,i}\sqrt{\left(\frac{\sigma_i}{D_{MEAS,i}}\right)^2 + \left(\frac{\delta(c_k)}{c_k}\right)^2}, \tag{20}$$

where $\sigma_i$ is the standard error in $D_{MEAS,i}$.

## 2.4 Screen measurements

### 2.4.1 BTV monitors with OTR screens

There are four *monitor TV* (MTV) systems in the TT2: MTV.201, MTV.218, MTV.229 and MTV.241. They are comprised [8] of a camera and a set of several *optical transition radiation* (OTR) screens and filters, which can be inserted into the transfer line one at a time. Each screen has its own unique material composition and thickness.

When a beam passes through one of the screens, light is emitted. This light can then be detected by the cameras, which record each active screen upon illumination. The cameras encode each image into a text file in the .sdds format. This format contains the pixel values in addition to tags such as camera/screen specifications and time of capture. The image can then be decoded during post-processing to reconstruct the beam image.

Depending on the beam intensity and the screen material, a filter might be overlayed the screen to achieve a certain transmission value. Choosing a filter with a too high transmission value can cause the camera to become saturated, leading to distortion in the beam image. On the other hand, a too low transmission value results in a low signal to noise ratio, rendering the image indiscernable.

The video gain can also be toggled with, in order to achieve a wider dynamic range of values.

| Date | 30.01.13 |
|---|---|
| Beam type | 25 ns LHC-type |
| Kinetic energy [GeV] | 26 |
| Intensity [ppb] | $1.2 \cdot 10^{-4}$ |
| $\epsilon_l$ [eVs] | 0.31 |
| $\epsilon_{NORM,X} \cong \epsilon_{NORM,Y} [\mu mrad]$ | 2.5 |
| No. of bunches | 12 |
| Bunch rotation? | No |
| Bump setting | Old |
| Momentum spread $\Delta p/p$ | $2.5 \cdot 10^{-4}$ |
| Error in momentum spread $\delta(\Delta p/p)$ | $3.1 \cdot 10^{-6}$ |

Table 5: Beam used during the screen measurement campaign.

### 2.4.2 Screen measurement procedure

For the screen measurements, four screens were employed in the TT2. 60 shots were taken per monitor with the old bump extraction conditions, using the beam in Table 5.

| MTV system | Axis | $\sigma_{MEAS,i}[mm]$ | $\delta(\sigma_{MEAS,i})[mm]$ | $D_{fit,i}[m]$ | $\delta(D_{fit,i})[m]$ | $\sigma_D^2/\sigma_{MEAS,i}^2$ |
|---|---|---|---|---|---|---|
| MTV.201 | X | 2.19 | $3.2 \cdot 10^{-2}$ | -3.25 | $2.6 \cdot 10^{-2}$ | 14% |
| MTV.218 | X | 1.73 | $1.9 \cdot 10^{-2}$ | -2.813 | $4.8 \cdot 10^{-3}$ | 17% |
| MTV.229 | X | 1.51 | $1.6 \cdot 10^{-2}$ | -1.22 | $1.5 \cdot 10^{-2}$ | 4% |
| MTV.241 | X | 1.34 | $1.8 \cdot 10^{-2}$ | 1.35 | $1.6 \cdot 10^{-2}$ | 7% |
| MTV.201 | Y | 1.47 | $1.4 \cdot 10^{-2}$ | -0.222 | $1.5 \cdot 10^{-3}$ | 0.2% |
| MTV.218 | Y | 1.37 | $2.0 \cdot 10^{-2}$ | 1.000 | $3.9 \cdot 10^{-3}$ | 3.4% |
| MTV.229 | Y | 1.61 | $2.4 \cdot 10^{-2}$ | 0.887 | $3.6 \cdot 10^{-3}$ | 2.0% |
| MTV.241 | Y | 1.54 | $6.3 \cdot 10^{-2}$ | 0.263 | $2.2 \cdot 10^{-3}$ | 0.2% |

Table 6: The terms which Equation 25 is comprised of, for each MTV system $i$.

### 2.4.3 Post-processing of screen data

Consider a screen in one of the monitors, at location $i$. The goal is to characterize the beam passing through the screen by image analysis. Assuming a 2D-Gaussian beam, one can calculate the *beam size* $\sigma_{i,p}$ in each plane at time $p$. The average beam size for a given monitor is then the average of the set $\{\sigma_{i,p}\}$ for a given $i$, with a standard deviation of $\delta(\sigma_i)$. With a set of beam sizes $\{\sigma_i\}$ and a reading of the momentum spread $\Delta p/p$, it is possible to reconstruct the betatronic parameters $(\alpha_0, \beta_0)$ at extraction from the PS. An estimate of the emittance $\epsilon$ can also be found.

For the actual image analysis one can refer to [7]. The main points are summarized here. Note that this procedure also requires dispersion

data. The propagated dispersion $D_{PROP,i}$ from Equation 19 will be used to estimate the dispersion values at the screen locations.

The image is initially reconstructed from the .sdds file. This can be performed by copying the pixel intensities from the .sdds file into a 2x2 matrix. The image is then overlayed a reference screen image, obtained from the measurement campaign or from [5]. The reference image is taken with the same camera as the ones used in the MTVs, but with a zoomed-out setting to capture the screen edges. These edges act as reference points used for calibration.

Figure 3 portrays an active screen in an MTV system, subject to a particle beam. To account for the free passage of the beam, geometry dictates that the camera has to view the screen at an angle (here $2\phi$) with respect to the beam. A projection procedure must be performed on the raw image to compensate for the angle. The procedure is documented in [7]. It involves remapping all the pixel values to different noninteger coordinates, then distributing the pixel values onto a rectangular grid. Calibration data [5] is then used to correlate the image lengths with real space lengths, as the reference screen appears as a rectangle on the rectified screen.

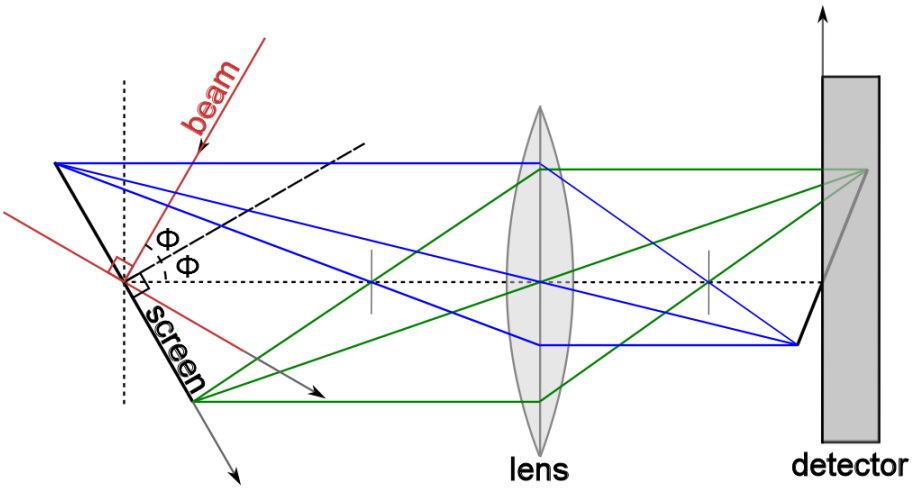


Figure 3: The camera detector and lens with respect to the MTV screen for a given MTV system. The green and blue rays represent rays of light through the optical system.

Finally, a Gaussian fit is performed. The image is initially projected onto both axes, and fit with a 1D function using Matlab. The function used for fitting is a Gaussian with a linear term:

$$f(x, a_1, a_2, a_3, a_4, a_5) = a_1 \exp\left\{\left(\frac{x - a_2}{a_3}\right)^2\right\} + a_4 + x a_5. \quad (21)$$

and similarly for y. The linear term is included to account for background noise.

From this fit the beam size $a_3$ is extracted, as it represents the spread of the beam shape.

The whole procedure is then repeated for the set $\{\sigma_{i,p}\}$ for all monitors $i$ for all times $p$ in both planes, and an average value of the spread is obtained along with the standard deviation. The result is the beam size in Equation 4, $\sigma_{RMS,i} \equiv \sigma_i$, and the corresponding standard deviation $\delta(\sigma_i)$.

### 2.4.4 Parameter reconstruction

With a set of $\sigma_i$ and $D_{FIT,i}$-values for several screens $i = 1 - 4$ in the transfer line, one can reconstruct the dispersion at extraction from the PS ($i = 0$). This is achieved by using the sine- and cosinelike parameters of each monitor location and a minimization scheme reminiscent of that of Equation 14. The procedure is described in [2]. In the following analysis the axis indices $(x, y)$ have been omitted for simplicity.

A least error function is constructed, which represents the difference in the measured and reconstructed beam sizes. The square of the reconstructed beam size is given by:

$$\sigma^2_{PROP,i} = \epsilon\beta_{PROP} = \epsilon(C_i^2\beta_0 + 2C_iS_i\alpha_0 + S_i^2\gamma_0) \quad (22)$$

where $C_i$ and $S_i$ are the sinelike and cosinelike parameters taken at point $i$, obtained from MAD-X. $\epsilon$ is the beam emittance, set to be constant throughout the system. $\gamma_0$ is a function of the other betatronic parameters at extraction [15]:

$$\gamma_0 = \frac{1 + \alpha_0^2}{\beta_0} \quad (23)$$

The corresponding $\chi$-function then becomes:

$$\chi_\beta = \sum_{i=1}^{4} \left(\frac{\sigma^2_{\beta,i} - \sigma^2_{PROP,i}}{\Delta_i}\right)^2 \quad (24)$$

$\sigma_{\beta,i}$ is given by moving Equation 4 around:

$$\sigma^2_{\beta,i} = \sigma^2_{MEAS,i} - \sigma^2_{D,i}, \quad (25)$$

The measurement results which make up the terms in Equation 25 are listed in Table 6. $\sigma^2_{D,i}$ refers to the product of $D_{FIT,i}$ and $\frac{\Delta p}{p}$, squared.

The weights $\Delta_i$ are obtained from using the Gaussian law of error propagation on $\sigma^2_{\beta,i}$:

$$\delta(\sigma^2_{\beta,i}) \equiv \Delta_i = 2\sqrt{\delta^2(\sigma_{MEAS,i})\sigma^2_{MEAS,i} + \delta^2(D_i)D_i^2\left(\frac{\Delta p}{p}\right)^4 + D_i^4\delta^2\left(\frac{\Delta p}{p}\right)\left(\frac{\Delta p}{p}\right)^2}. \tag{26}$$

Solving for the betatronic parameters at extraction can be performed by finding the global minimum of $\chi_\beta$ through a matrix minimization scheme:

$$\left\{\frac{\partial \chi_\beta}{\partial B_i} = 0\right\}, B_i \in \{\epsilon\alpha, \epsilon\beta, \epsilon\gamma\} \tag{27}$$

The function is minimized separately for each axis, as we assume no coupling. One can set up a system of equations:

$$\tilde{\mathbf{M}}\vec{x} = \vec{b}, \tag{28}$$

such that $\vec{x}$ is the vector of unknowns, $\vec{b}$ is a vector of constants and $\tilde{\mathbf{M}}$ is an invertible square matrix.

After solving Equation 28 for $\vec{x} = \{\epsilon\alpha, \epsilon\beta, \epsilon\gamma\}^T$, one can solve for $\epsilon$ by rearranging Equation 23 into:

$$\epsilon = \sqrt{(\epsilon\gamma_0)(\epsilon\beta_0) - (\epsilon\alpha_0)^2} \tag{29}$$

Finally, the betatronic functions are given by simple division by $\epsilon$.

### 2.4.5 Errors in the betatronic parameters

Errors in the fit parameters can be extracted from $\tilde{\mathbf{M}}$ in Equation 28. Denoting the variable $i$ in $\vec{x}$ as $x_i$, $i \in [1-3]$, the diagonal terms of the inverse matrix [2] refer to the statistical errors:

$$\delta(x_i) = \sqrt{\tilde{M}^{-1}_{i,i}} \tag{30}$$

Using the Gaussian formula for error propagation on Equation 29, one can obtain the error in the emittance:

$$\delta^2(\epsilon) = \frac{\delta^2(\epsilon\beta_0)(\epsilon\gamma_0)^2 + \delta^2(\epsilon\gamma_0)(\epsilon\beta_0)^2 + 4\delta^2(\epsilon\alpha_0)(\epsilon\alpha_0)^2}{4\epsilon^2}, \tag{31}$$

as well as the errors in $\beta$ and $\alpha$:

$$\delta^2(\beta_0) = \beta_0^2\left\{\left(\frac{\delta(\epsilon\beta_0)}{\epsilon\beta_0}\right)^2 + \left(\frac{\delta(\epsilon)}{\epsilon}\right)^2\right\}, \tag{32a}$$

$$\delta^2(\alpha_0) = \alpha_0^2\left\{\left(\frac{\delta(\epsilon\alpha_0)}{\epsilon\alpha_0}\right)^2 + \left(\frac{\delta(\epsilon)}{\epsilon}\right)^2\right\}. \tag{32b}$$

# 3 Results

## 3.1 Canonical solutions

The TT2-TT10 line is matched according to the canonical extraction parameters [3], listed in Table 7. Figures 4-7 show the dispersion and $\beta$-functions in the TT2-TT10 line and the SPS if one propagates these canonical values through the system with the MAD-X model.

| Canonical parameter | Horizontal value | Vertical value |
|---|---|---|
| $D[m]$ | 3.04 | 0.024 |
| $D'[1]$ | 0.253 | -0.014 |
| $\beta[m]$ | 26.14 | 10.88 |
| $\alpha[1]$ | -2.23 | 0.762 |

Table 7: The canonical dispersion and betatronic parameters, taken at extraction from the PS.

Because the matching criterion is met, the beam enters the SPS at $s = 1165$ with respect to the extraction point, with the correct injection conditions. Hence, the beam is well-behaved in the SPS, which can be seen by the sixfold symmetry in Figure 4. Every 1152 meters the dispersion repeats itself in the horizontal plane, which is given from the SPS design [10]. Such periodic behaviour is expected from stable circular accelerators [15]. Meanwhile, in the vertical plane, Figure 5 shows that the dispersion is eliminated at injection into the SPS. As both the PS and the SPS structures are positioned in the horizontal plane, there is no need for vertical bending magnets in the two rings. Hence, the vertical dispersion will stay unchanged in the SPS, which motivates a low value at injection.

The $\beta$-functions in the SPS behave even more systematically under the canonical extraction conditions, alternating between horizontal and vertical values in a FODO-pattern [10] just like the TT2-TT10 line. This is only possible if the injection conditions are met into the SPS, otherwise beating effects will start to appear. The plots of the $\beta$-functions using the canonical extraction parameters are given in Figures 6-7.

## 3.2 Dispersion results

Measurements were performed in the TT2-TT10 line and in the first turn of the SPS, in order to investigate drifts in the betatronic and dispersive extraction parameters from the PS with respect to the canonical values. Two different extraction conditions were compared in the dispersion measurement campaign, so that the quality of a new bump setting in the PS could be assessed. The measurements were performed in November 2012 and January 2013 using a 26 GeV LHC-type beam, specified in Table 3.

Beam position data was collected using BPMs in the TT2-TT10 line

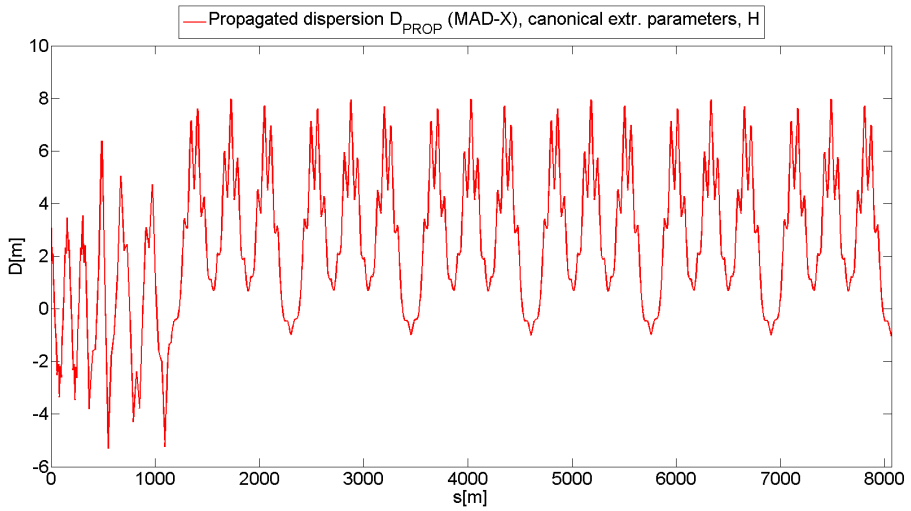


Figure 4: **A horizontal dispersion model propagated through the TT2-TT10 line and in the first turn of the SPS, using the canonical extraction conditions as input.**

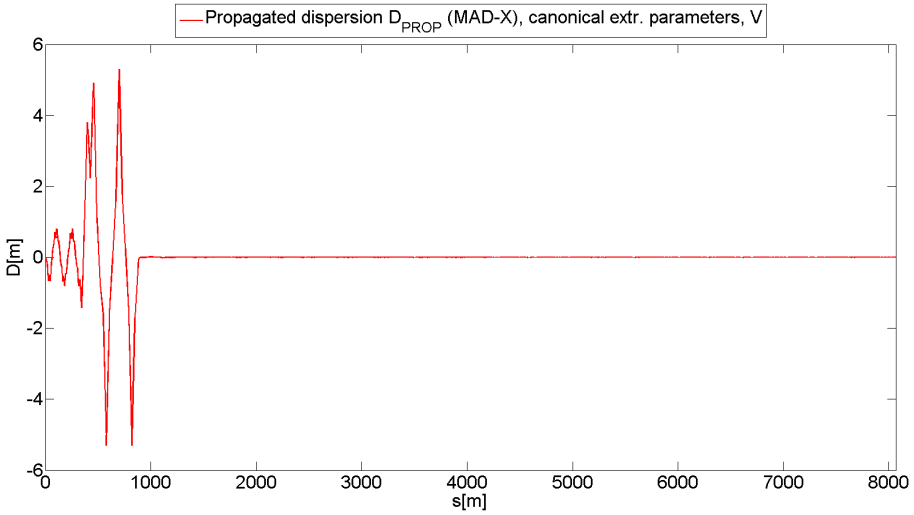


Figure 5: **A vertical dispersion model propagated through the TT2-TT10 line and in the first turn of the SPS, using the canonical extraction conditions as input.**

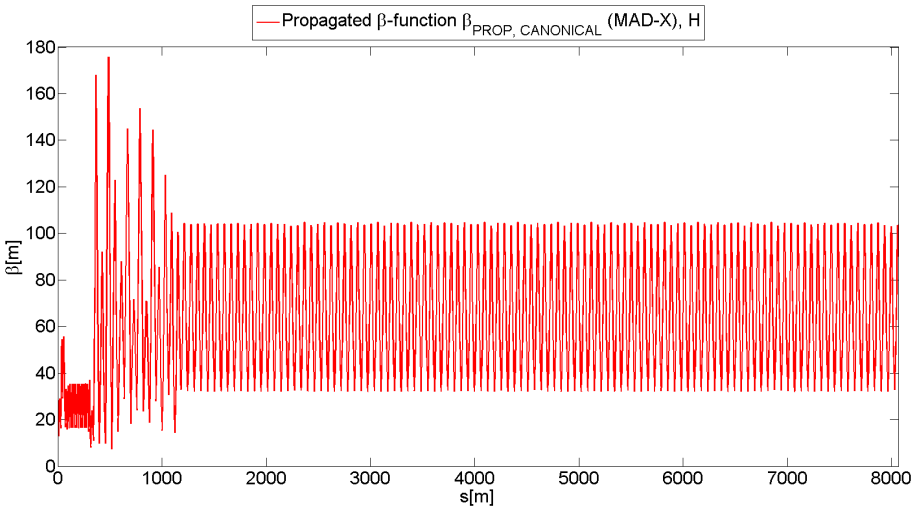


Figure 6: **A horizontal $\beta$-function model propagated through the TT2-TT10 line and in the first turn of the SPS, using the canonical extraction conditions as input.**

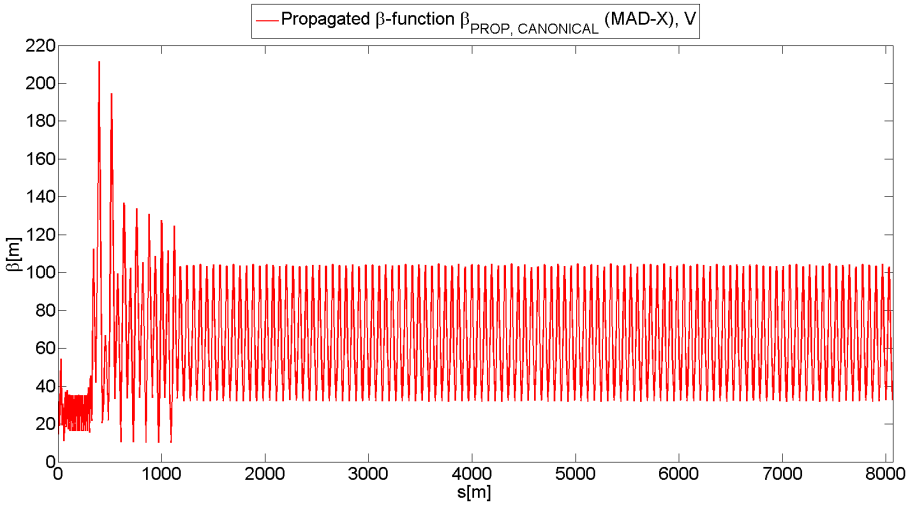


Figure 7: **A vertical $\beta$-function model propagated through the TT2-TT10 line and in the first turn of the SPS, using the canonical extraction conditions as input.**

and in the SPS. The total number of BPMs used in the analysis is specified in Table 8.

| Axis | Bump setting | Number of BPMs |
|---|---|---|
| X | New | 97 |
| Y | New | 90 |
| X | Old | 92 |
| Y | Old | 92 |

Table 8: The total number of BPM measurements used in the dispersion analysis for calculating the dispersion parameters at extraction from the PS. The numbers were taken after a cut in the threshold (Section 2.3.3) had taken place.

The data was used to produce a set of dispersion data by varying the momentum spread of the input beam. A new set of extraction conditions $\{D_0, D'_0\}$ was then calculated in both planes, through a least square error scheme in Microsoft Excel. The method minimized the difference between the measured and the propagated dispersion, the latter modeled in MAD-X [14]. The results are displayed in Tables 9-10, for both planes and extraction conditions.

| Dispersion parameter | Value | Error |
|---|---|---|
| $D_X[m]$ | 3.679 | $5.3 \cdot 10^{-3}$ |
| $D'_X[1]$ | 0.2900 | $5.8 \cdot 10^{-4}$ |
| $D_Y[m]$ | -0.105 | $1.2 \cdot 10^{-3}$ |
| $D'_Y[1]$ | -0.0130 | $1.4 \cdot 10^{-4}$ |

Table 9: Dispersion parameters calculated for the extraction point from the PS, based on data obtained under the new bump extraction condition.

| Dispersion parameter | Value | Error |
|---|---|---|
| $D_X[m]$ | 3.809 | $5.9 \cdot 10^{-3}$ |
| $D'_X[1]$ | 0.3048 | $6.2 \cdot 10^{-4}$ |
| $D_Y[m]$ | -0.178 | $1.5 \cdot 10^{-3}$ |
| $D'_Y[1]$ | -0.0047 | $1.5 \cdot 10^{-4}$ |

Table 10: Dispersion parameters calculated for the extraction point from the PS, based on data obtained under the old bump extraction condition.

These extraction parameters were then propagated through the TT2-TT10 line and the first turn of the SPS, using MAD-X software. This in turn confirmed the validity of the model by comparing the propagated fit to the measured points. The result is shown for both bump settings in both planes in Figures 8-11. The dispersion fits signal a break of the sixfold

symmetry of the SPS. Instead of recurring dispersion peaks of around 8 meters in Figure 4, the peaks alternate between 6 and 10 meters.

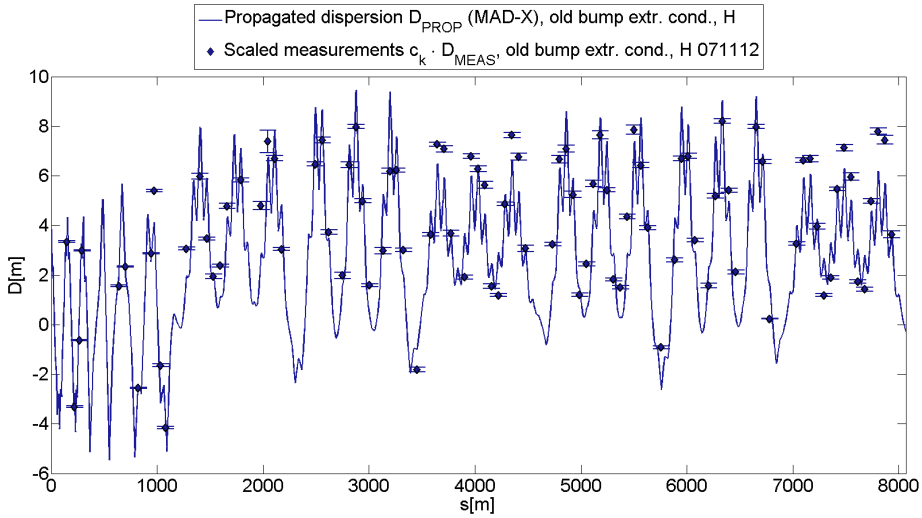


Figure 8: **Horizontal dispersion measurements taken in the TT2-TT10 line and in the first turn of the SPS, as well as a propagated dispersion fit, both subject to the old bump extraction settings.** The measured points are scaled by a calibration factor related to the local instrumentation.

Note that all of the measurement points are scaled by a calibration factor $c_k$, $k = \{TT2, TT10, SPS_H, SPS_V\}$ depending on the plane and location. This correction takes into account that the instrumentation systems in these separate areas are calibrated differently. The error bars of the points $\delta(c_k D_{MEAS})$ refer to the product of the two.

Table 11 lists all the calibration factors which were calculated simultaneously with the dispersion parameters at extraction from the PS. All of the factors are within 20% of 1, which is a sign that the values are reasonable. Furthermore, the two calibration factors pertaining to the SPS are within 2% of each other. In [2] these two calibration factors were treated as one single factor with good results. However, after recent discussions with Instrumentation [4], it was suggested that it is more correct to operate with two different factors for these BPMs, because of the way the electronics are laid out.

Table 12 showcases the differences in calculated extraction conditions, verifying that the values are very close. In the horizontal plane, these differences are on the order of 5%. In the vertical plane the values are very small, so a comparison using differences (in absolute units) is better. The difference in the vertical extraction parameters between bump settings is

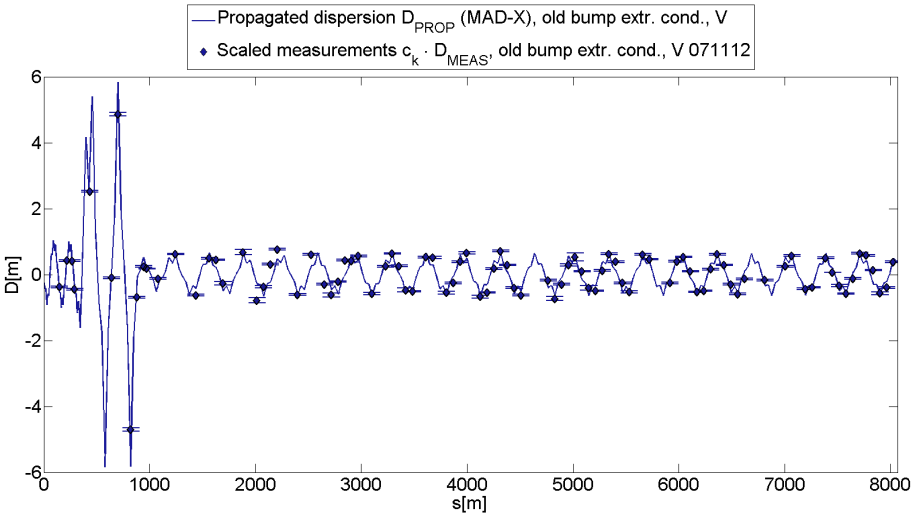


Figure 9: **Vertical dispersion measurements taken in the TT2-TT10 line and in the first turn of the SPS, as well as a propagated dispersion fit, both subject to the old bump extraction settings.** The measured points are scaled by a calibration factor related to the local instrumentation.

| Calibration factor | Value [1] | Error [1] |
|---|---|---|
| $c_{TT2}$ | 1.194 | $4.5 \cdot 10^{-3}$ |
| $c_{TT10}$ | 0.896 | $2.8 \cdot 10^{-3}$ |
| $c_{SPS,X}$ | 0.878 | $1.5 \cdot 10^{-3}$ |
| $c_{SPS,Y}$ | 0.861 | $4.2 \cdot 10^{-3}$ |

Table 11: The calibration factors calculated for each group of BPMs in the TT2-TT10 line and in the SPS.

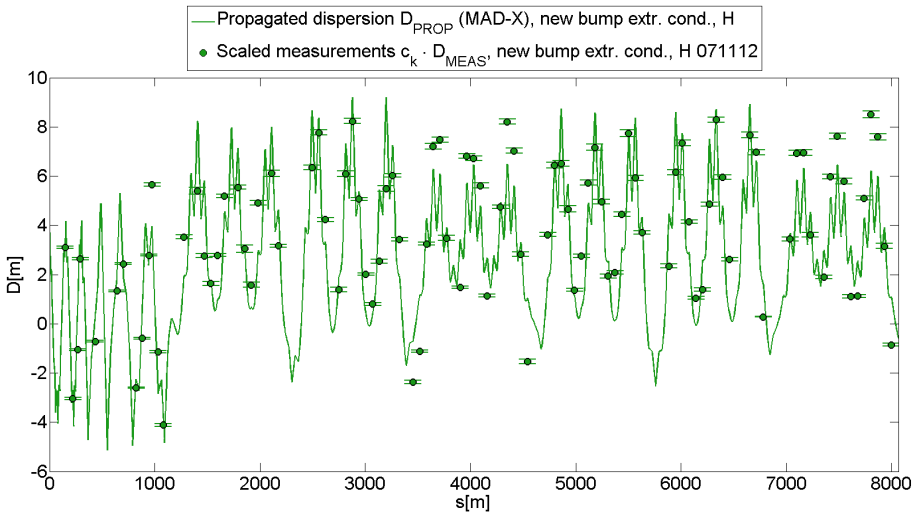


Figure 10: **Horizontal dispersion measurements taken in the TT2-TT10 line and in the first turn of the SPS, as well as a propagated dispersion fit, both subject to the new bump extraction settings.** The measured points are scaled by a calibration factor related to the local instrumentation.

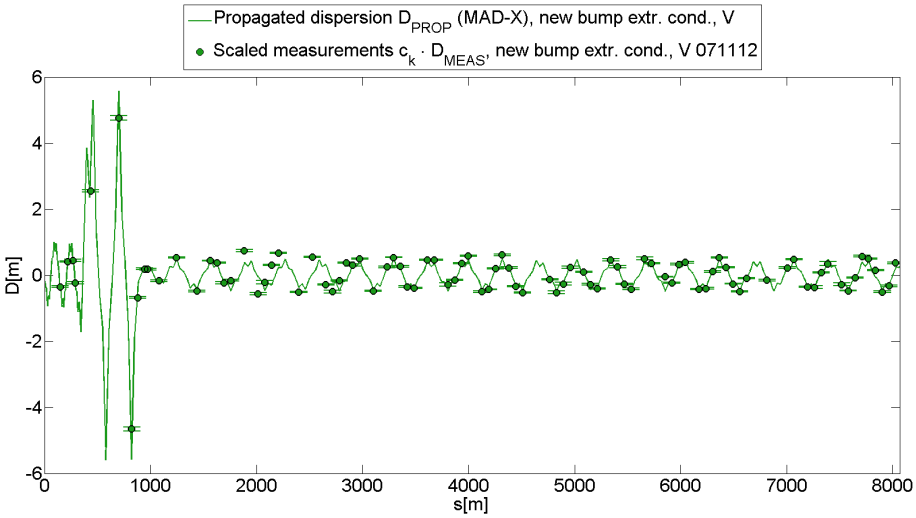


Figure 11: **Vertical dispersion measurements taken in the TT2-TT10 line and in the first turn of the SPS, as well as a propagated dispersion fit, both subject to the new bump extraction settings.** The measured points are scaled by a calibration factor related to the local instrumentation.

around half of the corresponding value found in the horizontal plane.

| Dispersion parameter | Difference (old-new) | Ratio ((old-new)/old) |
|---|---|---|
| $D_X[m]$ | 0.131 | 3.4 % |
| $D'_X[1]$ | 0.0148 | 4.9 % |
| $D_Y[m]$ | -0.073 | 41 % |
| $D'_Y[1]$ | 0.0082 | 174 % |

Table 12: Comparison between dispersion parameters obtained using different bump settings (old vs. new) in the PS.

This similarity in extraction parameters from the PS leads to similar propagated dispersion fits in the TT2-TT10 line and the SPS, as seen in Figures 12-13. Here the two dispersion fits are subtracted from each other, as they pass through the TT2-TT10 line and the first turn of the SPS. The difference is largest at injection into the SPS in the horizontal plane, with peak-to-peak differences of 0.8 meters. Then the difference stabilizes in the SPS, where the peak-to-peak differences go down to 0.6 meters. A comparable behaviour is found in the vertical plane, albeit with less peak-to-peak beating in the SPS than in the horizontal plane by 17%.

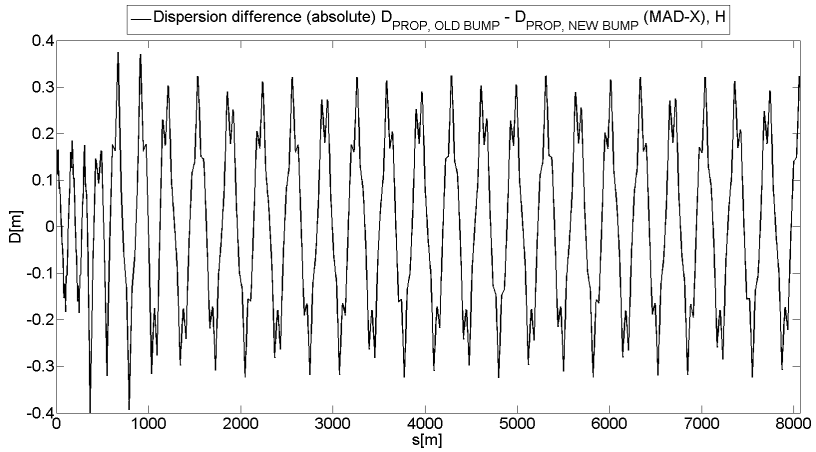


Figure 12: **The difference in the horizontal plane between two propagated dispersion functions in the TT2-TT10 line and the first turn of the SPS, where the two functions are calculated by starting with the old bump extraction parameters and the new bump extraction parameters respectively.**

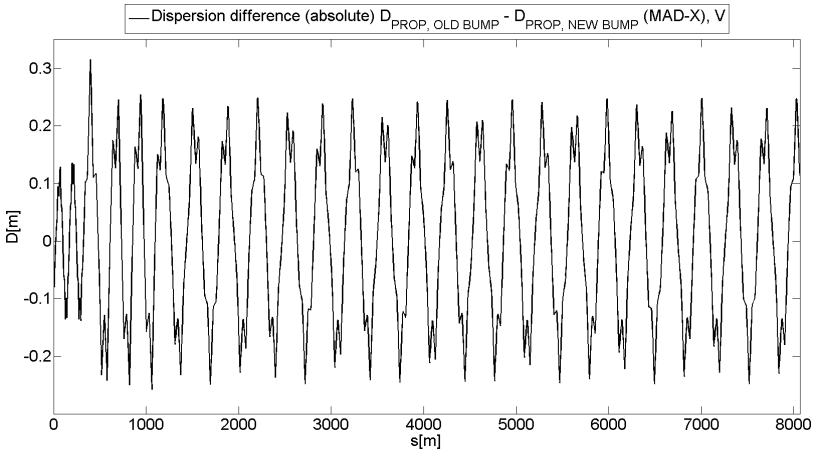


Figure 13: **The difference in the vertical plane between two propagated dispersion functions in the TT2-TT10 line and the first turn of the SPS, where the two functions are calculated by starting with the old bump extraction parameters and the new bump extraction parameters respectively.**

One can try to find the choice of extraction condition which produces the closest fit to the canonical extraction parameters. Table 13 lists the differences in the extraction parameters from the PS when one compares the recent results for the old and new bump extraction conditions with the canonical parameters.

| Parameter | Difference (new-can) | Ratio (new-can)/can | Difference (old-can)/can | Ratio (old-can) |
|---|---|---|---|---|
| $D_X[m]$ | 0.64 | 21.0 % | -0.77 | 25.2 % |
| $D'_X[1]$ | 0.037 | 14.8 % | -0.052 | 20.7 % |
| $D_Y[m]$ | -0.13 | 537 % | 0.20 | 842 % |
| $D'_Y[1]$ | 0.0011 | 7.49 % | -0.0093 | 66.3 % |

Table 13: Comparison between dispersion parameters calculated at extraction from the PS using the old and new extraction conditions and the canonical values from 2010

Figures 14-15 show how each fit compares to the canonical fits in the TT2-TT10-line and the SPS. The graphs confirm that which is stated in Table 13, namely that the new bump fits are actually closer to the canonical fits than the old bump fits in both planes. In the vertical plane, the peak-to-peak value of the difference at most is 0.8 m for the new bump comparison and 1.2 m for the old bump comparison, with the largest values of the discrepancy occuring in the SPS. Meanwhile, there is little difference in the horizontal plane as both bump settings lead to fits that are just as close to the canonical fits. The new bump fit is slightly closer, but only on the order of 0.1 m less peak-to-peak values with respect to the canonical fit.

## 3.3 Betatronic results

Screen data was collected using four MTV systems in the TT2, by subjecting them to a beam described in Table 5. The beam cross-sections were analyzed in Matlab to obtain the beam sizes in both transverse planes. The momentum spread was also measured. The old bump dipersion fits as well as the new bump dispersion fits from the previous analysis provided an estimate for the dispersion values at the screen locations.

This data was then synthesized into a beta-dependent beam size, which in turn was compared with a propagated beam size estimated with MAD-X optics data. An analytical least square minimization algorithm was constructed, which produced the betatronic parameters at extraction from the PS, along with the transverse emittances (Tables 14-16).

The betatronic parameters at extraction from the PS are extremely similar for the two choices of fitted dispersion values (old bump vs. new bump extraction setting), so only the old bump extraction setting will be compared to the canonical values.

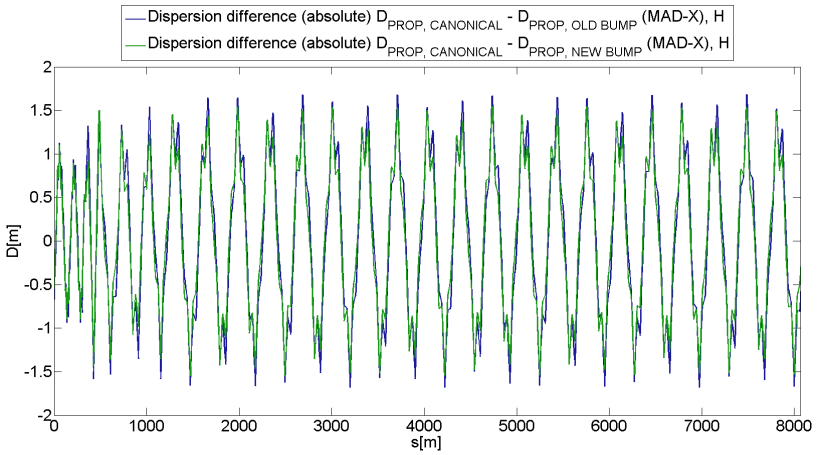


Figure 14: **The difference in the horizontal plane between the propagated dispersion functions in the TT2-TT10 line and the first turn of the SPS, calculated using the canonical extraction parameters from the PS, subtracting each of the two bump settings respectively.**

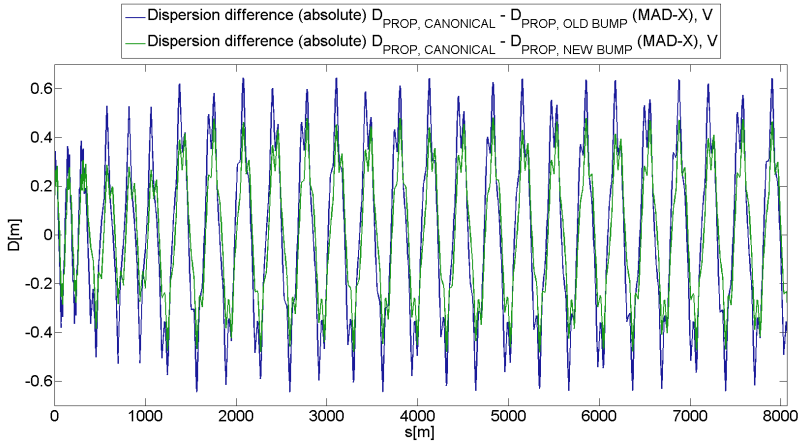


Figure 15: **The difference in the vertical plane between the propagated dispersion functions in the TT2-TT10 line and the first turn of the SPS, calculated using the canonical extraction parameters from the PS, subtracting each of the two bump settings respectively.**

| Betatronic parameter | Value | Error |
|---|---|---|
| $\beta_X[m]$ | 30 | 8.8 |
| $\alpha_X[1]$ | -2.7 | 0.81 |
| $\beta[m]$ | 14 | 1.5 |
| $\alpha_Y[1]$ | 1.5 | 0.16 |

Table 14: Betatronic parameters calculated using screen measurements and fitted dispersion data from old bump extraction conditions.

| Betatronic parameter | Value | Error |
|---|---|---|
| $\beta_X[m]$ | 30 | 8.9 |
| $\alpha_X[1]$ | -2.8 | 0.82 |
| $\beta[m]$ | 14 | 1.5 |
| $\alpha_Y[1]$ | 1.5 | 0.16 |

Table 15: Betatronic parameters calculated using screen measurements and fitted dispersion data from new bump extraction conditions.

| Axis | Bump setting | Normalized value $[\mu m]$ | Error $[\mu m]$ |
|---|---|---|---|
| X | Old | 3.3 | 0.97 |
| Y | Old | 2.4 | 0.25 |
| X | New | 3.3 | 0.98 |
| Y | New | 2.4 | 0.24 |

Table 16: Normalized transverse emittance $\epsilon_{NORM,n} = \beta_{REL}\gamma_{REL}\epsilon_n$, calculated for the 26 GeV beam in January 2013 (Table 5), for two different choices of extraction conditions.

To determine whether a drift had taken place in the betatronic values, $\beta(s)$-fits were propagated through the TT2-TT10 line and the first turn of the SPS, using the newly calculated betatronic extraction parameters from the PS as input. These fits were then compared with fits using the canonical betatronic values as input. Examining Figures 16-17 one can conclude that a clear difference in the $\beta$-function is present in both the TT2-TT10 line and in the SPS. The peak-to peak values in the SPS increase with 45 % in the horizontal plane and 114 % in the vertical plane. Furthermore, the FODO-symmetry of the SPS has been broken, as the $\beta$-peaks vary in height in both planes, between 80 and 120 m in the horizontal plane and between 50 and 170 meters in the vertical plane. The vertical $\beta$-function with the newly calculaed betatronic parameters also display high spikes in the TT10 of 344 m in the vertical plane and 211 m in the horizontal plane.

| Parameter | Old bump values | Canonical values | Difference (old-can) | Ratio ((old-can)/can) |
|---|---|---|---|---|
| $\beta_X[m]$ | 30 | 26.1 | -3.9 | 15 % |
| $\alpha_X[1]$ | -2.7 | -2.2 | 0.47 | 21 % |
| $\beta_Y[m]$ | 14 | 10.9 | -3.1 | 29 % |
| $\alpha_Y[1]$ | 1.5 | 0.76 | -0.7 | 97 % |

Table 17: Comparison between betatronic parameters attained using screen measurements and the canonical values from 2010 [3].

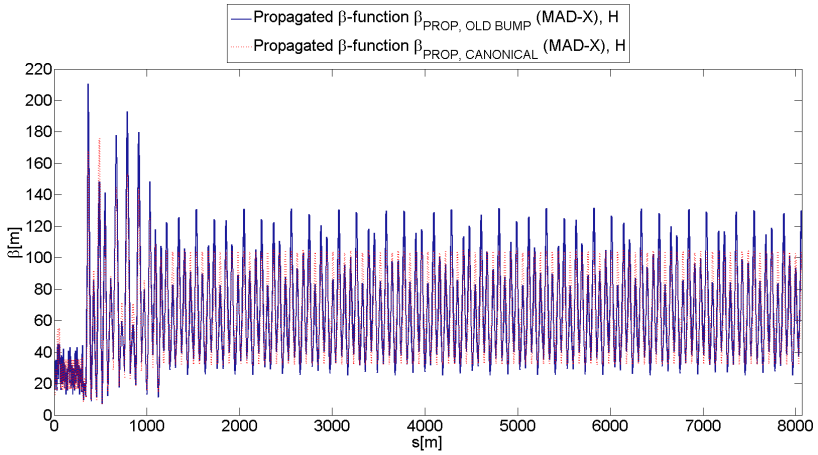


Figure 16: **Two propagated $\beta$-functions in the horizontal plane of the TT2-TT10 line and the first turn of the SPS, with the canonical set of extraction parameters and the old bump extraction parameters respectively.**

The betatronic extraction parameters from the PS for two different extraction settings are compared in Figures 18-19. In these two figures

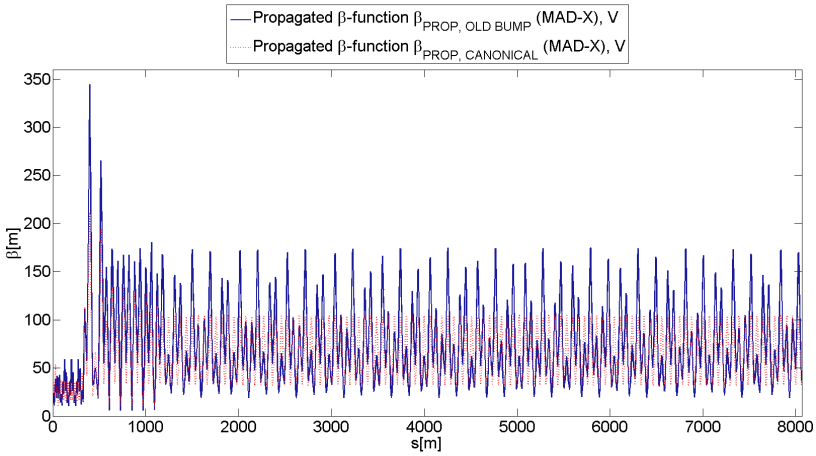


Figure 17: **Two propagated $\beta$-functions in the vertical plane of the TT2-TT10 line and the first turn of the SPS, with the canonical set of extraction parameters and the old bump extraction parameters respectively.**

the difference is propagated through the TT2-TT10 line and the first turn of the SPS. The difference in the propagated dispersion between the two bump settings is never larger than 2.1 meters in the horizontal plane and 0.9 meters in the vertical plane. These differences are two orders of magnitude lower than the average $\beta$-values extracted from the propagated fits in the SPS in both planes.

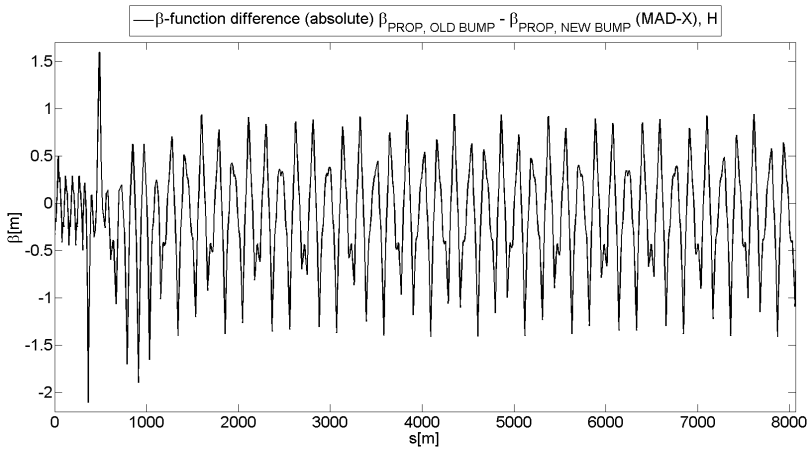


Figure 18: **The difference in the horizontal plane between two propagated $\beta$-functions in the TT2-TT10 line and the first turn of the SPS, where the two functions are calculated by propagating the old bump extraction parameters and the new bump extraction parameters respectively.**

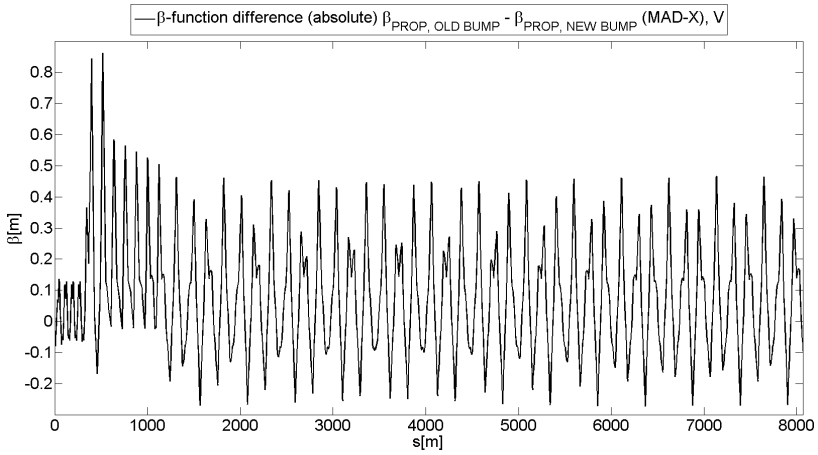


Figure 19: **The difference in the vertical plane between two propagated $\beta$-functions in the TT2-TT10 line and the first turn of the SPS, where the two functions are calculated by propagating the old bump extraction parameters and the new bump extraction parameters respectively.**

# 4 Discussion

It has been shown that there is a mismatch between the newly calculated dispersion parameters and the canonical parameters at extraction from the PS. In the following analysis the old bump extraction conditions will be assumed, as the main points of the discussion differ little by changing from the old bump to the new bump extraction conditions in the PS.

The discrepancy between the recently calculated extraction parameters and the canonical parameters has been found. In the horizontal plane the dispersion was found to be 0.8 meters lower than the matched solution, while in the vertical plane it was found that the dispersion had increased by 0.2 meters with respect to the canonical parameters.

This mismatch manifests as an irregular dispersion beating in the SPS in both planes. The sixfold symmetry in the horizontal plane of the SPS dispersion consists of six sets of curved sections, each comprised of 3 big dispersion oscillations [10]. These arc sections now display differences of 3.4 meters in peak heights between neighbouring arc sections. Furthermore, there is stray dispersion beating in the vertical plane of the SPS on the order of 1.2 meters peak-to-peak. In the properly injected SPS this dispersion beating is zero.

The betatronic functions have also been compromised. Mismatches in the $\beta$-functions at extraction from the PS has been found to be 4 meters in the horizontal plane and 3 meters in the vertical plane. This mismatch carries over into the TT2-TT10 transfer line, with additional $\beta$-beating of over 40 meters with respect to the canonical solution in the horizontal plane. The corresponding increase in beating in the vertical plane is at 130 meters, giving rise to $\beta$-peaks in the transfer line of almost 350 meters. The beta-functions carry over into the SPS, where the FODO-symmetry of the synchrotron [10] is broken in both planes. Irregular beating patterns appear with increases in the $\beta$-peaks, measured to be 60 meters in the vertical plane and 30 meters in the horizontal plane.

Since the $\beta$-values are set to be equal in terms of FODO-symmetry in the SPS, a sign of asymmetry in the $\beta$-values can suggest that a coupling effect has taken place. This can be attributed to the dissimilarity in measured emittance values. The vertical emittance is unchanged at around $2.5\mu m$, but the horizontal has increased by a factor of 38% to $3.3\mu m$. A coupling phenomenom between the horizontal and longitudinal planes can be the reason for this increase, which also raises the uncertainty in the measured betatronic parameters and the emittance in the horizontal plane by a factor of 3.

In addition, the extraction parameter calculation is very sensitive of values of the screen size, as this is the dominating term in Equation 25. The screen size term in the betatronic beam size dominates by 1-2 order of magnitudes over the dispersive term, as Table 6 showcases. Therefore, any systematic calibration errors in the screen measurements, in addition to coupling effects, will have a significant impact on the calculated extraction

parameters.

Hence, the hypothesis posed in the outset has been verified. The parameters drift naturally over time, due to changes in the accelerator structures upstream. Therefore, a drift in the dispersive and betatronic parameters at extraction was expected, after over 5 years since the last measurement campaign [2].

The results imply that is necessary to rematch the TT2-TT10 line in order to reach the proper injection conditions into the SPS. If this is not done, tails in the particle distribution will start to appear and sudden drops in beam performance will manifest. By changing the quadrupoles in the matching sections of the TT2-TT10 line [13], one can tailor the dispersion and the betatronic functions to both the extraction conditions from the PS and injection conditions into the SPS.

The outcome of the bump comparison will be affected by future matching campaigns. As the TT2-TT10 transfer line was not matched to the old bump extraction conditions from the outset, it is hard to quantify how close the propagated orbits of the new and old bump extraction parameters could have been post-matching. At any rate, the results show that comparing the propagated dispersion conditions through the TT2-TT10 transfer line and into the SPS, small differences in dispersion beating between the two bump settings can be discerned. In the horizontal plane, this difference in variation from the canonical solution is on the order of 0.6 meters in the horizontal plane and 0.4 meters in the vertical plane. In both planes the new bump setting is closest with respect to the canonical solution.

Comparing the betatronic variations when changing the bump settings at extraction from the PS, the analysis show that the variation in $\beta$-values in the SPS with bump setting is on the order of 2 meters in the horizontal plane, and 1 meter in the vertical plane.

In summary, it has been shown that the bump settings are practically interchangeable at this stage with respect to the propagation of dispersive and betatronic parameters from the PS to the SPS. As the new bump parameters are slightly closer to the canonical solution than the old bump parameters, it is recommended to nominate this setting as the default, at least until the next matching campaign has come to an end.

# References

[1] E. Benedetto. Optics measurements and matching of tt2-tt10 line for injection of the lhc beam in the sps. *CERN-AB-Note-2008-055 ABP, Cern, Geneva*, 2008.

[2] E. Benedetto. Initial twiss parameters for tt2 @ 26 gev/c fast extraction. *tt2_fe_26_2010.inp, available from the CERN optics repository*, 2010.

[3] C. Boccard. (private communication).

[4] S. Burger. (private communication).

[5] CERN. The 300 gev programme. *CERN - Service d'information informatique H/487 - 4000*, 1972.

[6] E. Bravin E. Benedetto. Calibration and correction of the btvs images. *CERN-AB-Note-2008-024 ABP, Cern, Geneva*, 2008.

[7] S. Burger et. al. E.Bravin. A new tv beam observation system for cern. *CERN-AB-2005-076 BDI, Cern, Geneva*, 2005.

[8] K. Fuchsberger. Novel concepts for optimization of the cern large hadron collider injection lines. *CERN-THESIS-2011-075, Vienna*, 2011.

[9] Y. Papaphilippou H. Bartosik, G. Arduini. Optics considerations for lowering transition energy in the sps. *CERN-ATS-2011-088, Cern, Geneva*, 2011.

[10] O.E. Berrig et. al. M.J. Barnes. The cern ps multi-turn extraction based on beam splitting in stable islands of transverse phase space. *CERN2006011, Cern, Geneva*, 2006.

[11] D. M. Oppenheimer. New and improved solver, September 2009. http://blogs.office.com/b/microsoft-excel/archive/2009/09/21/new-and-improved-solver.aspx.

[12] A. Ulsroed. New optimization schemes for the tt2-tt10 transfer line regarding accurate injection into the cern super proton synchrotron. *Project work, NTNU*, 2012.

[13] F. Schmidt W. Herr. A mad-x primer. *Tech report CERN-AB-2004-027-ABP, Cern, Geneva*, 2004.

[14] K. Wille. *The Physics of Particle Accelerators*. Oxford University Press, 2000.

# A Gaussian error propagation

A function $f(A_1, A_2, A_3, ..., A_L)$ has an error given by

$$\delta(f) = \sqrt{\sum_{l=1}^{L} \left( \frac{\partial f}{\partial A_l} \delta(A_l) \right)^2}, \tag{33}$$

where $\delta(A_l)$ is the error in parameter $A_l$.